Pivotal role of solid phase interactions for the pressure-induced bi-stability of cyanide-bridged Fe 2 Co 2 square complexes

Buqin Xu, Yanling Li, Geoffrey Gontard, Keevin Béneut, Paraskevas Parisiades, Maxime Deutsch, Rodrigue Lescouëzec

ARTICLE

Pivotal role of solid phase interactions for the pressure-induced bi-stability of cyanide-bridged Fe_2Co_2 square complexes

Buqin Xu,[a] Yanling Li*,[a] Geoffrey Gontard,[a] Keevin Béneut,[b] Paraskevas Parisiades,[b] Maxime Deutsch,[c] and Rodrigue Lescouëzec*[a]

Received 00th January 20xx,
Accepted 00th January 20xx

DOI: 10.1039/x0xx00000x

Cyanide-bridged FeCo coordination clusters, recognized as exceptional candidates for molecular switches, have been the subject of extensive research efforts aimed at unraveling the key factors governing the charge transfer process. Previously, we have observed that the square complex $\{[Fe(Tp)(CN)_3]_2[Co(vbik)_2]_2\}^{2+}$ with Tp = tris(pyrazolyl)borate and vbik = bis(1-vinyl-2-imidazolyl)ketone, abbreviated as $\{Fe_2Co_2\}$, undergoes thermal charge transfer in MeOH solution near room temperature allowing the obtention of a solvatomorph pair exhibiting distinct electronic configurations at 300 K: $\{Fe^{III}_2Co^{II}_2\}\cdot 2BF_4\cdot 2MeOH$ (**1**) and $\{Fe^{II}_2Co^{III}_2\}\cdot 2BF_4\cdot 10H_2O\cdot 2MeOH$ (**2**). While **2** keeps charge transfer ability in solid state, **1** is trapped in the paramagnetic state by solid phase interactions down to 2 K, which make it a good candidate for investigating electron transfer under hydrostatic pressure, an external stimulus scarcely used for these systems. In the present work, we demonstrated that the synthesis method can be used to obtain new solvatomorph with remarkable pressure-induced electron transfer. The paramagnetic $\{\{Fe^{III}_2Co^{II}_2\}\cdot 2(PF_6)\cdot 2MeOH$ (**3**) and the diamagnetic $\{[Fe^{II}_2Co^{III}_2\}\cdot 2(PF_6)\cdot nH_2O\cdot mMeOH$ (**4**), isostructural to **1** and **2** respectively, were obtained. The stronger intermolecular interactions due to the PF_6 anion leads to a greater distortion of the core structures of **3** and **4**, affecting their magnetic properties under ambient and hydrostatic pressure. Notably, **3** exhibits a partial pressure-induced conversion from a paramagnetic to a diamagnetic state followed by a back conversion above a pressure threshold value, which is rationalized by a symmetry-breaking phase transition at ca 0.96-1.0 GPa. This unusual behavior has been analyzed using magnetometry, X-ray diffraction, and μ-Raman spectroscopy under various pressures. A deeper understanding of the electron transfer process in **3** was achieved by analyzing its structural data under various pressures and comparing them to that of **1**. The distinct electron transfer behaviors observed in the two complexes are likely correlated to the differing distortions in their square core structures induced by pressure.

Introduction

Molecular switches have garnered significant interest for their potential applications in next-generation molecule-based switching devices.[1,2] Their ability to change their physical and mechanical properties in response to external stimuli makes them interesting candidates for the manufacturing of molecular-based information storage device, sensors and actuators.[3–5] Over the last two decades, bistable molecular counterparts of FeCo Prussian Blue Analogues have attracted increasing attention as molecular magnetic switches.[6–8] Under external stimuli such as light, temperature, pressure, electric field,[9] these cyanide-bridged coordination clusters can undergo intramolecular electron transfer coupled to a spin transition on the cobalt site (ETCST), converting thus the (Fe^{II}_{LS}–CN–Co^{III}_{LS}) state into (Fe^{III}_{LS}–CN–Co^{II}_{HS}) one. Among the FeCo coordination clusters, the most investigated compounds are cyanide-bridged Fe_2Co_2 complexes,[10,11] of general formula $\{[Fe(^RTp)(CN)_3]_2[Co(L)_2]_2\}(A)_2\cdot S$ (with ^RTp = tris(pyrazolyl)borate derivatives, L = α- or β-diimines, A = counter-anion and S = solvent). The two first Fe_2Co_2 square complexes were reported in 2010: $\{[Fe(Tp^*)(CN)_3]_2[Co(bpy)_2]_2\}\cdot(OTf)_2\cdot 4DMF\cdot 2H_2O$ with bpy = 2, 2′-bipyridine and OTf = trifluoromethanesulfonate, and $\{[Fe(pzTp)(CN)_3]_2[Co(^{Me}bik)_2]_2\}\cdot(ClO_4)_2\cdot 3H_2O$ with ^{pz}Tp = tetrakis(pyrazolyl)borate and ^{Me}bik = bis(1-methyl-2-imidazolyl)ketone.[12,13] Then, efforts have been focused on the control of the light-induced and thermally-activated ETCST process in the solid state. This control can be achieved by several ways: (i) the nature of the capping ligand ^RTp or L control the redox potential of the Fe and Co subunits, which are of prime importance for the switchable properties;[14–17] (ii) varying the

[a] Institut Parisien de Chimie moléculaire, CNRS UMR 8232, Sorbonne Université, 4 place Jussieu 75252 Paris cedex 5 (France)
[b] Institut de minéralogie, de physique des matériaux et de cosmochimie CNRS UMR 7590, Sorbonne Université, 4 place Jussieu 75252 Paris cedex 5 (France)
[c] CRM2, UMR 7036, Université de Lorraine–CNRS, BP 70239 Boulevard des Aiguillettes, F 54506, Vandœuvre-lès-Nancy (France)

Electronic Supplementary Information (ESI) available: [details of any supplementary information available should be included here]. See DOI: 10.1039/x0xx00000x

counter-anion may impact both the square core structure and the crystal packing, hence intermolecular interactions.[18,19] (iii) the formation of H-bonding between a donor and the free CN group on the Fe ion can alter the redox potential of iron site.[20–22] Compared to light and temperature, the use of pressure as external stimulus was rarely investigated on switchable FeCo complexes,[23] even though it was proved to be a very useful mean to control the spin transition (ST) of Fe^{II} based complexes[24,25] and ETCST transition in several PBAs coordination polymers.[26–28]

In the last years, our group has more specifically investigated a family of Fe_2Co_2 squares having the general formula $\{[Fe(^{R}Tp)(CN)_3]_2[Co(^{R}bik)_2]_2\}(A)_2\cdot S$ where ^{R}bik is a β-diimine. In our early work, we used ^{Me}bik as blocking ligand on Co site and obtained interesting ETCST Fe_2Co_2 squares, allowing for fundamental study on light- and temperature-activated ETCST.[13,29,30] However, the transition temperature of these squares is largely above the room temperature (350-400 K), limiting their potential applications. By replacing ^{Me}bik ligand by ^{v}bik [bis(1-vinyl-2-imidazolyl)ketone], we succeeded in lowering the ligand field around the Co^{II}_{HS} ion, stabilizing thus the $Fe^{III}Co^{II}$ paramagnetic state. This led to the obtention of the square complex $\{[Fe(Tp)(CN)_3]_2[Co(vbik)_2]_2\}\cdot(BF_4)_2$ showing ETCST transition in MeOH mother solution near room temperature (figure S6a).[31] By controlling the crystallization temperature, above and below the transition temperature, $T_{1/2}$, we isolated two solvatomorphs from the mother solution. A diamagnetic phase, $\{[Fe^{II}(Tp)(CN)_3]_2[Co^{III}(vbik)_2]_2\}(BF_4)_2\cdot 10H_2O\cdot$MeOH (**2**), was obtained at 5°C and a paramagnetic one, $\{[Fe(Tp)(CN)_3]_2[Co(vbik)_2]_2\}(BF_4)_2\cdot 2$MeOH (**1**), at 35°C. The green diamagnetic phase (complex **2**) shows an ETCST in the solid state with $T_{1/2}$ at about 330 K, while the red paramagnetic phase (complex **1**) appears paramagnetic in the temperature range of 2 - 400 K. Magnetic studies at low scan rate (*ca*. 0.01 K/min) actually revealed a kinetic trapping of the paramagnetic state, with a transition $T_{1/2}$ that is decreased to *ca* 140 K in the solid-state phase of **1**, about 200 K lower than that of **2**. We hypothesized that the stabilization of the paramagnetic state could be associated to stronger intermolecular interactions that lead to a higher distortion of the Co coordination sphere favoring the high-spin Co^{II} state. Moreover, complex **1** shows a thermally induced ETCST in solution and a kinetically trapped ETCST in the solid state, revealing a moderate energy gap between its paramagnetic and diamagnetic states. We assumed that it could be sensitive to pressure which could favor the diamagnetic state with lower volume. This has motivated our first pressure study on **1** that actually revealed a piezo-induced ETCST process. The pseudo-paramagnetic **1** can effectively be converted by moderate pressure in a diamagnetic state which is endowed with an unusual feature: the thermal bistability domain increases with increasing pressure (fig. S6b).[32] A further in-depth investigation of the pressure-induced ETCST transition of **1** at 300 K by synchrotron X-ray diffraction on single crystal permitted to probe the elastic properties of the square complex as a function of pressure, with an attempt at rationalizing the unusual behavior.[33] Firstly, the Grüneisen parameter (γ_G), which relates the stiffening of the compound to the volume change upon pressure application, was determined. The exceptionally high value extracted for γ_G (9.3) is indeed coherent with the prediction established by Spiering *et al.* By using a continuum mechanic model, they demonstrated that a high γ_G value exceeding 1.8 can result in atypical spin transition of Fe^{II} based complexes with thermal hysteresis width enhanced by pressure. Spiering's model gives thus a theoretical basis for the occurrence of the unusual behavior but it does not reveal its structural origin. Secondly, we investigated the linear bulk moduli *versus* pressure along the three crystallographic axes. We observed that the linear bulk moduli, which depict the stiffness of **1** in specific directions could be related to specific intermolecular interactions. In particular, the stiffest direction of the material (axis c) could be associated to short contacts between the cationic square and the counter-anions, revealing their ability to propagate elastic interactions. Interestingly, the linear bulk modulus in c direction does not vary monotonously with increasing pressure but goes through a maximum. A careful scrutiny of the crystal data reveals that this unusual variation could be associated to the distortion of the square core as pressure increases. Importantly, we clearly demonstrated that the indirect interactions between squares mediated by the BF_4^- anion is the primordial intermolecular interactions at ambient and low pressure (< 0.46 GPa). π – π stacking of the vbik ligands on Co ion only becomes dominant at higher pressure (> 0.46 GPa) once pressure-enhanced. This in-depth analysis reveals how intricate the response to pressure of such molecular materials can be.

In the present work, we aim to answer the questions that have been raised by our previous studies. Is it possible to obtain other solvatomorphs with different electronic configurations by controlling the crystallization temperature? Is it possible to create new phases blocked in paramagnetic state? Would they be sensitive to pressure? If so, is the behavior under pressure going to be atypical? To answer these questions, we selected another counter anion, the octahedral PF_6^- in place of the tetrahedral BF_4^-. We thus intend to keep the $T_{1/2}$ of the square complex close to room temperature in MeOH solution, in order to ease the obtention of two crystal phases by controlling the crystallization temperature. By doing so, we also aim to investigate further the impact of subtle changes in the crystal structure on the switchable properties.

In this paper, we present the synthesis and characterizations of two solvatomorph squares compounds: $\{[Fe(Tp)(CN)_3]_2[Co(vbik)_2]_2\}(PF_6)_2\cdot 2$MeOH (**3**), a red paramagnetic complex and $\{[Fe(Tp)(CN)_3]_2[Co(vbik)_2]_2\}(PF_6)_2\cdot n$ Solvent (**4**), a green complex. At ambient pressure, **3** and **4** were characterized using X-ray diffraction measurements on single crystal (SC-XRD) and by variable temperature magnetization measurements. These results facilitated the establishment of a relationship between the core structure and the ETCST property for the related square complexes **1**-**4**. Moreover, the thermal electron transfer coupled spin transition (ETCST) and the symmetry-breaking phase transition of complex **3** under pressure were thoroughly investigated using high-pressure (HP) magnetic measurements, HP single-crystal X-ray diffraction (HP-SC-XRD), and HP Raman spectroscopy. The comparison of ETCST behaviors between complexes **3** and **1**, along with their

respective structural modifications under varying pressures, provides valuable insights into the unusual ETCST of complex **3** and underlines the crucial role of the counter-anion in solid-phase interactions.

Results and discussion

Structures and magnetic properties of 3 and 4 at ambient pressure

Crystal structures of **3** and **4** determined by SC-XRD analysis at 200 K are shown in fig. 1a and 1b. Both compounds, crystallized in triclinic group *P-1*, are isostructural to **1** and **2** respectively. Selected crystallographic data and structural parameters are given in the tables S1 and S2. To facilitate the structural analysis, it is necessary to specify that the two vbik ligands on Co site are not crystallographically equivalent. They are named vbik1 and vbik2 respectively, according to the labelling of their O atoms. In the crystal packing of **1**-**4**, it is vbik ligand bearing polar carbonyl group which plays an active role by building strong supramolecular interactions instead of Tp ligand.

As previously observed for **1**, the paramagnetic **3** shows a distorted core structure featured by two bent NC-Co angle (∠C1N1-Co = 167.1° and ∠C1N1-Co = 159.3°) and a ∑Co value of 38.1° (∑Co is the sum of the deviation from 90° of the twelve cis N-Co-N angles around Co site). The vbik ligands in **3** adopt a near planar conformation characterized by small dihedral angles between imidazole rings of each ligand (8.8° and 11.7°) and by two almost straight Co-C=O angles (175.4° and 174.0°). At ambient pressure, complex **3** shows supramolecular structures very similar to **1**, with the same types of intermolecular interactions.[32] The π - π stackings of vbik1-pair and vbik2-pair organize the squares into a layer (fig. S3). The vbik1-pair stacking propagates along the a direction, while vbik2-pair stacking, in the [0 1 1] direction. The counter-anions connect the squares of different layers through short contacts along a chain in the c direction. In order to have a quantitative view of the short contacts, the Hirshfeld surface analysis[34,35] was carried out and compared to that reported for **1** (fig. S5). In brief, the replacement of BF_4^- by PF_6^- increases the intensity of overall intermolecular interactions in **3** (SI section). This conclusion comes from the following three observations: (i) the distance between the antiparallel C=O groups is shorter, leading to a more pronounced π - π stacking of the vbik1 in **3**; (ii) the distances of the short contacts in the π - π stacking of vbik2 in **3** are smaller and give red spots on the Hirshfeld surface at ambient pressure (table S3 and fig. S5); (iii) the PF_6^- in **3** forms more significant pseudo H-bonds between Tp and vbik ligands (table S4) and the average H···F distance is shorter in **3** than in **1**. The greater intensity of intermolecular interactions in **3** likely puts more strain on the geometry of square complex and could explain the more distorted coordination sphere of the Co site in complex **3** (∑Co = 38.1°) compared to **1** ((∑Co = 35.1°).

In a similar way as **2**, the crystal cell of **4** contains two distinct squares, **4a** and **4b**, oriented in different directions. Both squares have rather regular core structure: the four NC-Co angles are in the range of 172.1-174.1° The values of ∑Co are small, 18.4° for **4a** and 15.7° for **4b** (table S2). which is in agreement with the low-spin Co^{III} d^6 electronic configuration. The vbik ligand in **4** is much less planar than in **3**: the dihedral angles between imidazole rings are in the range of 23.3-28.4° and the Co-C=O angles vary from 160.5 to 162.9°. The crystal packing of **4** is similar to that of **2** which we previously described.[31] Complementary information common to both complexes can be found in the ESI section (Table S2 and figure S4).

The fig. 1c and 1d show the thermal variation of the product of the molar susceptibility (χ_M) and the temperature (T), for the compounds **3** and **4** respectively. As for **1**, **3** is paramagnetic in the temperature range 2-300 K (figure 1c). However, unlike **1**, the

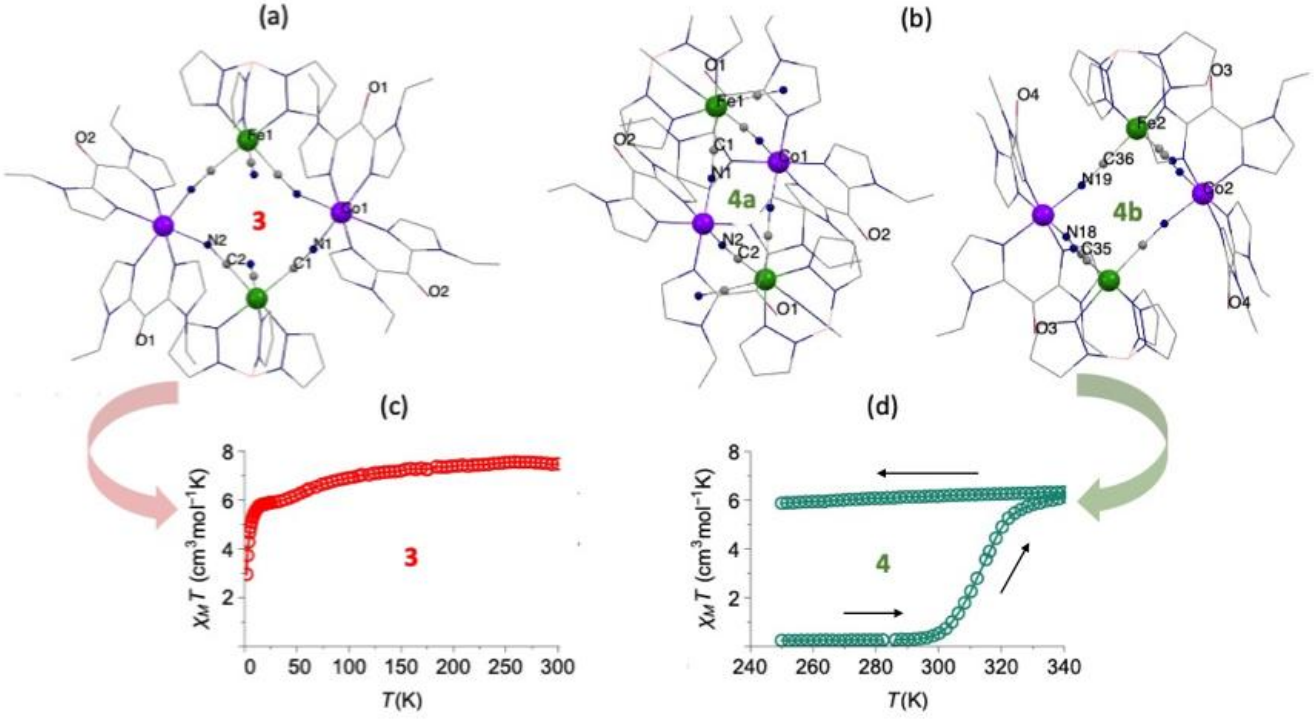

Fig. 1 Perspective view of the square complexes in **3** (a) and **4** (b) and thermal variation of $\chi_M T$ for **3** (c) and **4** (d) at ambient pressure. The arrows in fig. 4d indicate the direction of temperature change.

magnetic measurements at slow scan rate of 0.01 K/min did not reveal kinetically hindered thermal ETCST, which points to a better stabilization of the paramagnetic state in **3** than in **1**. The $\chi_M T$ value at 300 K is 7.53 cm^3 mol^{-1} K, matching with the expected value of two magnetically independent Fe^{III}_{LS} ions (S= 1/2, g ≈ 2.3-2.7)[36–38] and two Co^{II}_{HS} ions (S=3/2, $\chi_M T$ = 2.6-3.3 $cm^3 mol^{-1} K$).[39] Upon cooling, the $\chi_M T$ value diminishes slightly due to the spin-orbit coupling (SCO) effects in both Fe^{III}_{LS} and Co^{II}_{HS} ions. It reaches a pseudo plateau of ca. 5.9 cm^3 mol^{-1} K in the temperature range of 30 - 10 K. Below 10 K, $\chi_M T$ value drops from 5.5 to 2.95 cm^3 mol^{-1} K at 2 K owing to the combined effects of antiferromagnetic intermolecular interactions and of magnetic anisotropy of **3**. Compound **4** has a very similar ETCST behavior than **2**. In diamagnetic state for T < 290 K ($\chi_M T$ = 0.25 cm^3 mol^{-1} K), it undergoes an irreversible thermal ETCST transition at *ca.* 315 K, lower than 325 K for **2** and its $\chi_M T$ reaches 6.33 cm^3 mol^{-1} K at 340 K (figure 1b), smaller than that of **3** at 300 K, nevertheless still in the range of $\chi_M T$ values reported for Fe_2Co_2 squares in paramagnetic state.[37]

The differences in the magnetic properties of the squares **1** and **3** and of the squares **2** and **4** can be related to the distortion of the square core structure. In particular, two parameters have been highlighted in the literature to influence the electronic state: the distortion of the cobalt coordination sphere, ∑Co, and the distortion of the Fe-NC-Co bridges represented by the average Co-NC angle. It is expected that deviation of the coordination sphere from the ideal octahedral geometry weakens the metal-ligand bonding orbital interactions and lead to weaker ligand field, therefore stabilizing a HS Co(II) state.[37] Actually, the effects of ∑Co on the ETCST properties were studied by Liu T *et al*. for a five-membered family of tetranuclear complexes, $\{[Fe(pzTp)(CN)_3]_2[Co(dpq)_2]_2\}\cdot(A)_2$ with pzTp = tetrakis(pyrazolyl)borate, dpq = dipyrido[3,2-d:2',3'-f]quinoxaline and A = BF_4^-, PF_6^-, OTf^- and $\{[Fe(pzTp)(CN)_3]^-$. They demonstrated experimentally and theoretically that a strong ∑Co value stabilizes the paramagnetic state of the Fe-CN-Co pair.[18] On the other hand, there is no specific report in the literature about the effects of the Fe-CN-Co distortion on the ETCST of the FeCo coordination clusters. However, Bleuzen et *al*. measured the ligand field strength at the Co(II) site in two Prussian Blue analogues (PBAs) using X-ray absorption spectroscopy: $Co^{II}_4[Fe^{III}(CN)_6]_{2.7}\square_{1.3}\cdot 18H_2O$ and $Rb_{1.8}Co^{III}_{3.3}Co^{II}_{0.7}[Fe^{II}(CN)_6]_{3.3}\square_{0.7}\cdot 13H_2O$ (where □ represents vacancies). They observed that the ligand field at the Co(II) site in both PBAs is significantly weaker than the values typically reported for octahedral high-spin Co(II) coordination compounds. This reduction in crystal field strength was attributed to distortion in the Co-CN linkage, caused by strain within the PBAs structure. In fact, the linear conformation of Co–NC entities is associated with stronger orbital interactions between Co and the CN^- ligand, resulting in a stronger ligand field at Co. In contrast, bending of the Co-NC moieties disrupts this orbital interaction, leading to a weaker ligand field.[40]

It is therefore interesting to compare the distortion parameters of the square core and the ETCST properties of the complexes **1**-**4**, summarized in the table 1. The average distortion of Fe-CN-Co linkage (av. ∠CoNC) is similar for **2** and **4** on one side, and for **1** and **3** on other side and does not seem to play a critical role in the present case. More interestingly, the magnetic properties of these squares appear sensitive to the distortion of the coordination environment of Co site. As previously observed in the literature, a greater value of ΣCo stabilises the high spin Co^{II} state and thus stabilizes **3** in its paramagnetic state compared to **1**. Reciprocally, the lower distorted coordination sphere of the low-spin Co^{III} ion in **2** compared to **4** may account for a better stabilization of the low-spin state and a higher transition temperature.

Table 1. The distortion parameters of square core and magnetic properties of **1-4**.

Square	Av. ∠CoNC (°)	ΣCo(°)	$T_{1/2}$ (K)	Reference
2	173.06	16.21	325	31
4	172.20	18.44	315	this work
1	163.51	35.08	Kinetically trapped ETCST	31
3	163.21	38.06	Paramagnetic	this work

Magnetic measurements under various hydrostatic pressures

As mentioned above, the stronger distortion in the Co coordination sphere in **3** with comparison to **1** is coherent with a better stabilization of the paramagnetic state. The magnetic measurement realized at ambient pressure actually indicates that the paramagnetic state is either the ground state, or eventually a metastable state which would be more efficiently blocked than in **1** (i.e. with a lower $T_{1/2}$ that would require even lower scan rate measurement to be detected). In any case, **3** appears as a good candidate for pressure study, since the ETCST observed in solution and in the solid phase **4** indicate that the energy difference between the dia- and para-magnetic state is small and the application of moderate pressure could permit to trigger the switching toward the diamagnetic state with smaller volume. As a matter of fact, the magnetic behaviour of **3** is strongly affected by the application of hydrostatic pressure as shown in fig. 2. A pressure greater than *ca*. 0.39 GPa leads a partial conversion of paramagnetic pairs into diamagnetic ones in **3**. The molar fraction of paramagnetic species unconverted by pressure, γ_{para}, can be estimated by calculating the ratio of the $\chi_M T$ value at 150 K over that at 300 K: γ_{para} = $\chi_M T$ (150K) / $\chi_M T$ (300K). The pressure-induced diamagnetic pairs then undergo a thermally-activated ETCST upon heating with hysteresis opening. Depending on the pressure range, below or above a threshold value of *ca*. 0.6 GPa, two distinct behaviours can be observed. First of all, in the low-pressure range, below *ca*. 0.60 GPa, the degree of paramagnetic-to-diamagnetic conversion of **3** raises progressively with increasing pressure to reach a maximum of *ca.* 50 % at p = 0.59 GPa. The diamagnetic pairs induced by the hydrostatic pressure can be converted back to the paramagnetic state by increasing the temperature as shown in figure 2a. Interestingly, large hysteresis with width, $\Delta T_{1/2}$, of 50-20 K are

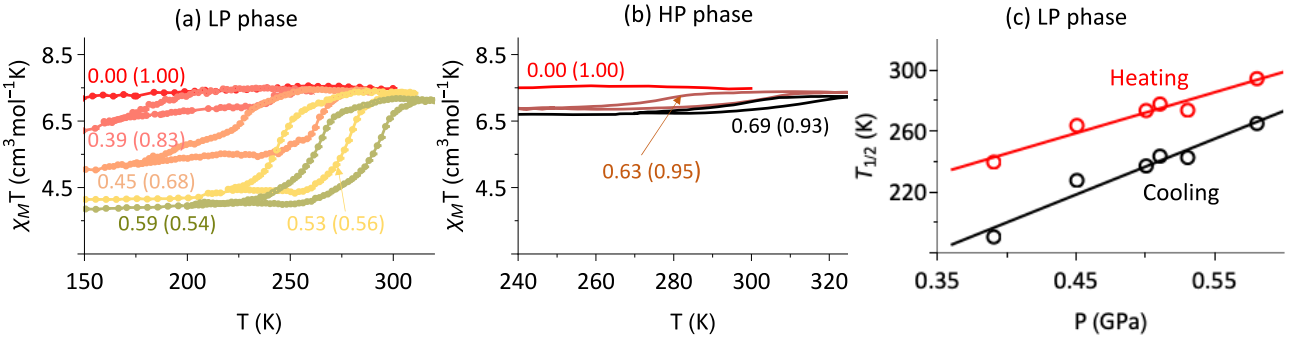

Fig. 2 (a) $\chi_M T$ versus T for low-pressure (LP) phase of 3, (b $\chi_M T$ versus T for high-pressure (HP) phase, and (c) Transition temperature versus pressure for LP phase at heating and cooling. The numbers in a and b indicate the pressures in GPa corresponding to each $\chi_M T$ - T curve and the numbers in bracket, and the molar fraction of paramagnetic species unconverted by pressure, γ_{para}, [$\gamma_{para} = \chi_M T$ (150K) $\chi_M T$ (300K)].

observed. In contrast with what was observed in **1**, $\Delta T_{1/2}$, decreases as the pressure increases, which corresponds to the normal behaviour usually observed in spin-crossover and switchable metal-metal charge-transfer complexes (*e.g.* FeCo PBAs).[26] Surprisingly, by applying a pressure of 0.63 GPa, the paramagnetic pairs are recovered: γ_{para} raises suddenly to 0.95 and only a marginal amount (5 %) of **3** show a thermal ETCST at heating temperature $T_{1/2}\uparrow$ = 301 K and cooling temperature $T_{1/2}\downarrow$ = 279 K with a smaller hysteresis ($\Delta T_{1/2}$ = 22 K). The fig. 2b shows the new trend of the thermal variation of $\chi_M T$ for **3** in the high pressure (HP) range. With further pressure increasing to 0.69 GPa, the γ_{para} value decreases slightly to 0.93. Concomitantly the thermal ETCST transition temperatures still shift upward to reach $T_{1/2}\uparrow$ = 312 K and $T_{1/2}\downarrow$ = 296 K ($\Delta T_{1/2}$ =16 K). When the pressure is released below 0.60 GPa, the compound **3** recovers its ETCST behaviour observed at low-pressure, and the process is reversible.

The fig. 2c shows that the transition temperatures measured upon heating and cooling, $T_{1/2}\uparrow$ and $T_{1/2}\downarrow$, versus pressure obeys to Clapeyron's law in the low-pressure regime:

$$T_{1/2}(p) = T_{1/2}(0) - (p - p_0)\,\Delta V/\Delta S \quad (1)$$

where ΔV *and* ΔS (both positive) are respectively the volume and entropy change between diamagnetic and paramagnetic states; $T_{1/2}(0)$ is the transition temperature corresponding to the threshold pressure p_0 beyond which ETCST transition takes place. At low temperature γ_{para} versus p data can be fitted to a polynomial equation of second order: $\gamma_{para} = 2.461 - 6.064\,p + 4.748\,p^2$ (fig. S6). The extrapolation of this equation to $\gamma_{para} = 1$ gives an estimation of p_0 = 0.32 GPa. This is coherent with our experimental measurments.

The linear regression of $T_{1/2}$ versus p data gives two equations for $T_{1/2}\uparrow$ and $T_{1/2}\downarrow$ respectively:

$$T_{1/2}\uparrow = 138.95 + 267.19\,p \ (R = 0.97327) \quad (2)$$

$$T_{1/2}\downarrow = 54.66 + 365.08\,p \ (R = 0.97417) \quad (3)$$

The shift of $T_{1/2}$ to higher temperature is expected, since the pressure leads to a stabilization of the diamagnetic state. The table 2 compares the $\Delta V/\Delta S$ values of **3**, **1**, some FeCo PBAs and selected SCO complexes for heating and cooling. This table shows that the two Fe_2Co_2 squares have significantly higher $\Delta V/\Delta S$ ratio than both the corresponding FeCo PBA coordination polymers[41] and the SCO complexes.[24,25] These square molecules appear thus more sensitive to pressure than the last two types of switchable compounds.

1. HP-SC-XRD evidence of the phase transition

In order to rationalize the unusual pressure dependent magnetic behaviour of **3**, we devoted some efforts to carry out HP-XRD measurements at 300 K on single crystals. Actually, these experiments are challenging since the crystalline quality of **3** decreases rapidly when removing crystals from the mother solution. This loss of crystallinity forced us to start measurements before the pressure had completely stabilized. To quantify the pressure shift, we systematically measured the pressure before and after the XRD measurement (approx. 18 hours). The experimental procedure of XRD on two single crystals of **3** called SC1 and SC2 respectively are detailledd in SI section. The measurements were performed by increasing the pressure from 0 to 1.77 GPa on SC1, and by decreasing pressure from 1.60 to 0.05 GPa on SC2. The selected crystal data and structural refinement are summarized in the table S4 in SI section.

Table 2. Comparaison of the *ΔV/ΔS* values for **3**, **1**, FeCo PBAs and SCO complexes of Fe(II).

Compound	**ΔV/ΔS (K/GPa)**		**Reference**
	Heating	Cooling	
3	280.9	315.3	present work
1	228.4	213.6	31
$K_{0.1}Co_4[Fe(CN)_6]_{2.7}\cdot 18H_2O$	170	25	41
SCO complexes of Fe(II)	100-200	24	24, 25

When increasing the pressure on the crystal SC1, we detected a phase transition between 0.76(2) GPa and 1.55(25) GPa (see cell parameters at both pressure in table S4). Due to the decrease of crystallinity after the phase transition, the crystal structure of the high-pressure phase, $\mathbf{3_{HP}}$, could not be solved. We thus applied a

pressure of 1.60(5) GPa on a second crystal (SC2) and attempted to perform HP-SC-XRD measurements immediately before significant deterioration of crystal quality. Unfortunately, the structural resolution was not possible because of the too low number of reliable independent diffraction peaks for $\mathbf{3_{HP}}$ which has a lower symmetry than $\mathbf{3_{LP}}$. Actually, the comparison of the diffractograms of SC2 before and after the phase transition, as illustrated in the fig. 3, allows the identification of the new diffraction peaks in the HP phase showing a doubling of the lattice in direct space. Moreover, the $\mathbf{3_{LP}}$ structure can be expressed in a non-conventional triclinic setting *I-1* with cell parameters close to $\mathbf{3_{HP}}$ lattice, as showed in the table 3. Therefore, the phase transition results in a loss of centering vector which can be obtained by a slight reorganization of the molecules in the crystal packing. This indicates that the $\mathbf{3_{HP}}$ space group type is a k-subgroup of the $\mathbf{3_{LP}}$ one. Interestingly, by lowering the pressure on

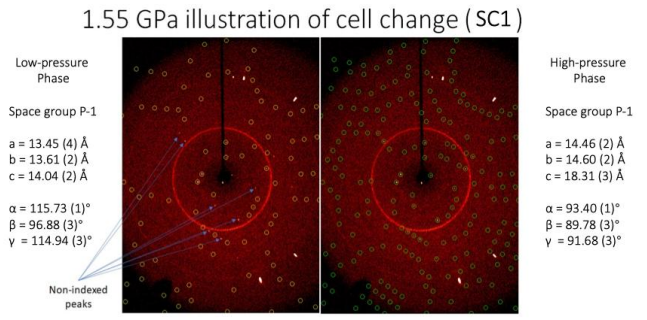

Fig. 3 Diffraction patterns of **3** (SC1) at 1.55 GPa indexed with the low-pressure phase (image a) and the high-pressure phase with doubled lattice volume (image b).

SC2 we obtained again the low-pressure phase, $\mathbf{3_{LP}}$, showing that the phase transition is reversible. The measurements on the crystal SC2 also allow to identify more precisely the pressure range in which the transition takes place, *i.e.* between 0.96(2) GPa and 1.15(5) GPa (figure S8).

Table 3. Illustration of the phase transition with non-conventional setting.

Pressure (GPa)	0.76(2)	0.76(2)	1.55(25)
Crystal system, Space group	Triclinic, $P\bar{1}$	Triclinic unconventional $I\bar{1}$	Triclinic, $P\bar{1}$
a (Å)	13.3813 (12)	14.4506	14.46(2)
b (Å)	13.838 (8)	15.292	14.596(17)
c (Å)	14.288 (8)	18.325	18.31(3)
α(°)	114.146(12)	93.83	93.40(6)
β(°)	97.12(2)	91.38	89.78(7)
γ(°)	115.89(2)	91.57	91.68(6)
Z'	0.5	1	1
Volume (Å^3)	2019(2)	4038	3855.(15)
V/Z'	4038	4038	3855

The symmetry-breaking phase transition observed by HP-SC-XRD in the pressure range of 0.96 - 1.15 GPa is actually the same one detected by HP magnetometry in the pressure interval of 0.59 – 0.63 GPa. The discrepancy of the transition pressure obtained by the two methods is due to the fact that the pressure is measured at very different temperatures and in different set-ups. The pressure measured at 300 K for HP-SC-XRD experiments (based on ruby luminescence) can be considered as the most acurate one. On the contrary, for HP magnetometry the pressure is measured between 6 and 7.2 K based on the shift of superconductive transition temperature of lead, and it increases with temperature. A study of the pressure evolution *versus* temperature in Daphne oil (the pressure transmitting medium for magnetic measurements) shows that an initial low-temperature pressure between 0.35 and 0.67 GPa could be increased by 0.15-0.19 GPa at 300 K.[42] The real pressure of the phase transition at 300 K given by HP magnetometry could be estimated to be in the range of 0.74 - 0.82 GPa, near that given by HP-SC-XRD.

2. Pressure-induced modification of the core structure of **3**

The use of a diamond anvil cell (DAC) limits severely the data completeness of HP-SC-XRD measurements, leading to structural data of limited quality. For example, for the core structure of **3**, the error is estimated to be in the range of 4.2-6.1% for the determination of the M-L length, and in the range of 3.9-7.5% for that of the two Co-NC angles. In comparison, the errors of these two structural parameters are less than 0.4 % for the SC-XRD measurements at 200 K without DAC. In spite of the large experimental error, a linear regression analysis on all the structural data obtained on SC1, SC2, and on the single crystal measured at 200 K without DAC (named SC0) allowed to bring out the pressure-induced core structural modification of $\mathbf{3_{LP}}$. The figure 4 shows several core structural parameters plotted against pressure: the average metal-ligand length (M-L) of the Fe-CN-Co linkage (Co-N_{bridge} and Fe-C_{bridge}) and that of Co-N_{vbik} and Fe-N_{Tp} (fig. 4b); the angles ∠CoN1C1 and ∠CoN1C1 (fig. 4c) describing the distortion of the Co-NC-Fe linkages; ∑Co (fig. 4d) and ∑Fe (fig. 4e) accounting for the distortion of the coordination sphere of the two metal sites. Firstly, all the four types of M-L bond length display a linear decreasing trend with increasing pressure (details in SI), and that of the bridging CN ligand, Fe-C_{bridge} and Co-N_{bridge}, seem to be reduced much more rapidly than that of Fe-C_{Tp} and Co-N_{vbic}. Secondly, it seems that the pressure alters little the Fe-C1N1-Co linkage and bends mainly the Fe-C2N2-Co one: under increasing pressure (Fig 4c), Regarding the distortion parameters of the coordination sphere, ∑Co, it seems that its value oscillates around 38-39° for pressure equal or greater than 0.45 GPa, even though the poor quality of structural data leaves doubts about its sudden rise at 0.05. On the other hand, ∑Fe seems to go through a maximum between 0.5-0.6 GPa with increasing pressure.

As we suggested that the unusual ETCST behavior of **1** could originate from its core structural distortion upon pressure application. It is interesting to compare the pressure-induced deformation of the core structures of **1** and **3** (fig. S9) regarding the Fe-CN-Co linkages and the coordination spheres of the metallic ions. At first, there is a common point between the two complexes:

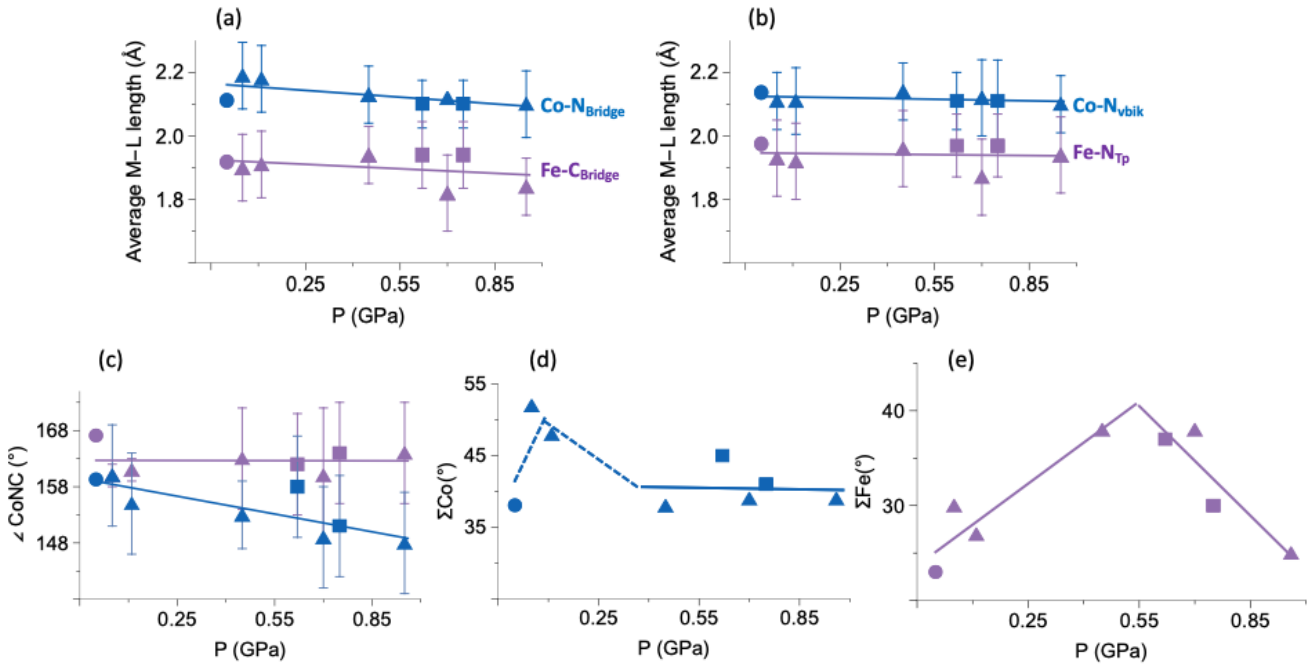

Fig. 4 Core structural parameters against pressure at 300 K of three single crystals of $\mathbf{3_{LP}}$ (disk = SC0, square= SC1 and triangle = SC2). (a) Average M-L length of Co-N_{Bridge} and of Fe-C_{Bridge}. The solid lines are the linear regressions of the experimental data 2.16 -0.071 p for Co-N_{Bridge} and 1.92 -0.047 p for Fe-C_{Bridge}. (b) Average M-L length of Co-N_{vbik} and of Fe-N_{Tp}. The solid lines are the linear regressions of the experimental data (2.12 - 0.016 p for Co-N_{vbik} and 1.95 -0.009 p for Fe-N_{Tp}). (c) The evolution of the angles CoN1C1 and CoN2C2. The solid lines are the linear regressions of the experimental data (162.68 -0.091 p for ∠CoN1C1 and 158.96 – 10.56 p for ∠CoN2C2). (d) Distortion parameter of Co site ΣCo. The dashed and solid lines are for eye-guide. (e) Distortion parameter of Fe site ΣFe. The solid line is for eye-guide.

the Fe-C1N1-Co linkage is much slightly affected by pressure than the Fe-C2N2-Co linkage. Aside from this common feature, the variation of other core structural parameters *versus* pressure is in strong contrast between **1** and **3**: i) the C2N2-Co angle ceases to decrease in **1** before 0.31 GPa, whereas that in 3_{LP} it keeps decreasing until 0.96 GPa; ii) the ∑Co value of **1** shows a moderate increase (*ca.* 2.6°) upon pressure application and keeps a constant value of about 36° between 0.18-0.46 GPa before the ETCST transition. While the ∑Co value of **3** is significantly above that of **1** in the pressure range of 0 -
0.96 GPa; iii) the ∑Fe value of **1** rises abruptly from 25° at ambient pressure to 34° at about 0.20 GPa before a decreasing to 25° at 0.31 GPa and then keeps this value till 0.95 GPa, whereas that of $\mathbf{3_{LP}}$ seems to rises linearly with pressure from 23°, before reaching a maximum value of 38° between 0.5-0.6 GPa and then decreases linearly. It is also observed that the ∑Co versus p curve for $\mathbf{3_{LP}}$ is always above that for **1**, indicating a more important distortion of the coordination sphere of Co ion in $\mathbf{3_{LP}}$ during pressure application.

This comparison permits the following assumptions about the ETCST behaviors of $\mathbf{3_{LP}}$ under pressure. A pronounced distortion of the coordination sphere of Co ion along with a continuous twist of Fe-C2N2-Co likely allows keeping $\mathbf{3_{LP}}$ in paramagnetic state. The overall higher ∑Co value of **3** in the LP phase might explain its higher pressure-threshold (p_0) for the para-to-dia conversion. The value of p_0 for **1** is about 0.10 GPa and that for **3**, about 0.32 GPa which were determined at low temperature (T = 6-7 K). Furthermore, in contrast to **1**, **3** has a normal ETCST behaviour featured by the decreasing thermal hysteresis width with increasing pressure. We are tempted to assume that the different distortion patterns of the core structure of **1** and $\mathbf{3_{LP}}$ upon pressure application might play an important role on their respective ETCST properties. But this hypothesis should be validated by further pressure studies allowing the obtention of more accurate structural data on related Fe_2Co_2 squares.

HP-μ Raman measurements on single crystal at 200 K.

The Raman spectroscopy gives access to the stretching vibrations of cyanide that are sensitive to the valence and spin-state of the metallic ions it bridges.[43] Moreover this technique can be indicative of the pressure-induced crystal phase change.[44] For these raisons, the Raman spectra are often used for probing both spin-state transitions[45,46] and crystal phase[47,48] of cyanide-based materials. In the present work, HP-μ Raman measurements of **3** were recorded at 200 K, since the pressure dependence of the electron transfer is much higher at this temperature than at room temperature (see magnetic data above).

As shown in Figure 5a, at 0.30 GPa, $\mathbf{3_{LP}}$ is in a paramagnetic state since the peak at 2174 cm^{-1} is typical of bridging [{Fe^{III}_{LS}(μ-CN)Co^{II}_{HS}}] moiety. Moreover, the stretching B-H vibration of the Tp ligand is located at 2466 cm^{-1}, well below 2500 cm^{-1}, which is as expected for the [Fe(Tp)CN_3]$^-$ subunit with an Fe^{III} ion (above 2500 cm^{-1} with an Fe^{II} ion).[49–51] When the pressure increases progressively from 0.30 to 0.70 GPa, the intensity of both peaks at 2174 and 2466 cm^{-1} decreases gradually. This is due to the progressive conversion of the red paramagnetic $\mathbf{3_{LP}}$ into the green diamagnetic $\mathbf{3_{LP}}$, as observed by magnetic measurements under pressure. As the green

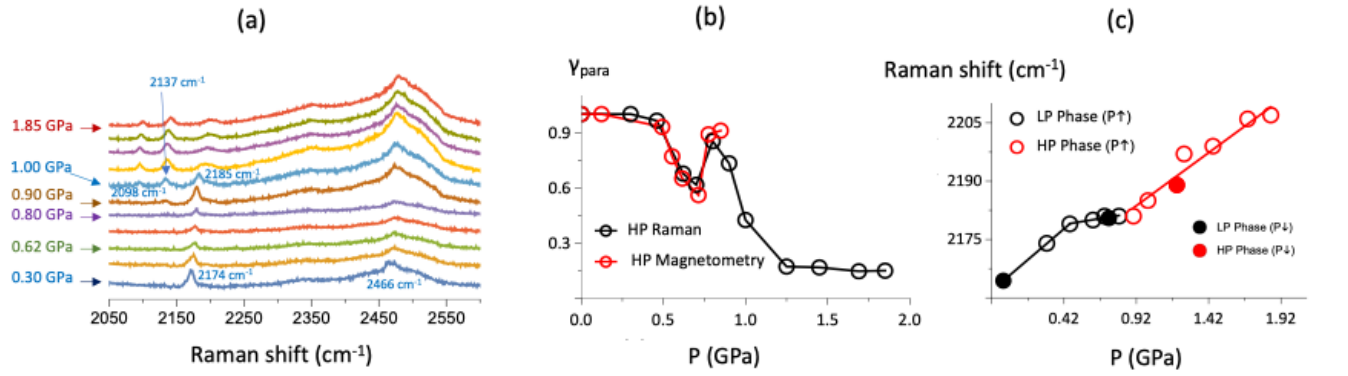

Fig. 5 (a) Raman spectra of **3** at 200K for pressure increasing from 0.3 to 1.85 GPa. (b) The paramagnetic molar fraction γ_{para} of **3** plotted against pressure at 200K deduced from Raman spectra (black circle), compared with that extracted from the magnetic measurements (red circle). The red curve is translated to higher pressure according to $p_{200} = 1.38 \times p_{LT} - 0.05$ (GPa) to take into account of the pressure increase with temperature. (c) Blue shift of the Fe^{III}-CN-Co^{II} stretching mode in **3** versus pressure. black circles represent Raman shift against pressure for low-pressure (LP) phase, and the red circles, for high-pressure (HP) phase. The solid lines are for eye-guide.

diamagnetic species absorbs the exciting laser light at 514.5 nm, the overall signal of **3** becomes weaker with increasing pressure. Interestingly, the signals of the diamagnetic Fe^{II}_{LS}(μ-CN)Co^{III}_{LS} and Fe^{II}-CN moieties in $\mathbf{3_{LP}}$ are absent in the Raman spectra till 0.80 GPa.[32] This suggests that the transition is cooperative with a transition front line separating well defined green/red crystal[52] and the green one absorbing laser light is Raman silent. This hypothesis is coherent with the magnetic behaviour showing hysteretic transition at moderate pressure and therefore strong cooperativity. Remarkably, from p = 0.90 GPa to higher pressures, the signature of diamagnetic pair appears with the occurrence of peaks located at 2137 and 2098 cm^{-1} assigned to the vibration of the bridging Fe^{II}-CN-Co^{III} cyanide group of **3**. We suspect here that the crystal phase transition detected in XRD may lead to a loss of crystallinity and a more gradual transition, for which the diamagnetic and paramagnetic pairs do no more form large defined crystalline domains but can be mixed. This would reduce the effect of the absorbance of the laser light.

In order to go further in the rationalization of these data, we proceed to a quantitative analysis of the Raman spectra to extract the γ_{para} versus pressure. At first, the vibration band of [{Fe^{III}_{LS}(μ-CN)Co^{II}_{HS}}] located at 2174-2203 cm^{-1} was integrated within adequate wavenumber interval to give the area $A_{CN}(p)$, which is proportional to the amount of paramagnetic pairs in the sample. Then the broad B-H stretching peak, considered as reference, was integrated from 2461 to 2599 cm^{-1} to take into account both Fe(II) and Fe(III) species (thus the total amount of diamagnetic and paramagnetic pairs). This gives the reference area $A_{BH}(p)$. The ratio of the two areas, $R(p) = A_{CN}(p)/A_{BH}(p)$ is proportional to the paramagnetic fraction $\gamma_{para}(p)$ at any pressure p. Knowing that $\gamma_{para}(0.30) = 1$, then $\gamma_{para}(p) = R(p)/R(0.30)$. The Figure 4b shows the curve of γ_{para} *versus* pressure obtained from Raman spectra, compared with that extracted from magnetic measurements at 200 K. Note that the later γ_{para} versus p curve is empirically translated to higher pressure according to $p_{200K} = 1.38 \times p_{LT} - 0.05$ (GPa), where p_{200} is the pressure estimated at 200 K and p_{LT}, the pressure determined at low-temperature (LT) between 6-7.2 K during the magnetic measurements. As mentioned above, according to several studies devoted to the pressure evolution with temperature in Daphne oil,[42,53,54] there is a linear relationship between the pressures at low and high temperatures. The discontinuity of both γ_{para}- p curves between 0.80 and 0.90 GPa is consistent with the occurrence of a crystallographic phase transition of **3** at 200 K. The slight difference of γ_{para} at 0.90 GPa given by the two methods comes certainly from the different samplings of the two methods: the magnetic measurements were performed on bulk sample while the Raman spectra, on single crystal. The HP-μ Raman measurements, allowing the application of pressure till 1.85 GPa, indicate that para-to-dia conversion of **3** reaches a plateau extent of *ca*. 75% at 200 K for pressure greater than 1.25 GPa.

Finally, the symmetry-breaking phase transition is also reflected in the variation against pressure of the Raman band blueshift of the {Fe(III)-CN-Co(II)} moiety, as showed by the fig. 5c. In $\mathbf{3_{LP}}$ phase, the blueshift of the cyanide bridge increases linearly upon pressure application and then slows down from 0.60 to 0.90 GPa. In 3_{HP} phase, the blueshift seems to increases linearly again with pressure.

Another feature of the HP Raman spectra (figure 4a) is that the band of [{Fe^{III}_{LS}(μ-CN)Co^{II}_{HS}}] (2174 – 2180 cm^{-1}), relatively sharp in low-pressure phase, broadens considerably in the high-pressure phase, which may be related to possible structural disorder of the moiety and a partial loss of cristallinity.[55]

In summary, the pressure-induced crystal phase transition of **3** can be revealed by two features in the evolution of the vibrations of [Fe^{III}-CN-Co^{II}] moiety versus pressure: the Raman intensity change and the regime change of the Raman shift. The results of Raman spectrometry indicate that the pressure onset for the crystallographic phase transition of **3** occurs near *ca* 0.90 GPa at 200 K, while it appears near ca. 0.96-1.15 GPa at 300 K according to the HP-SC-XRD measurements.

Conclusions

In conclusion, we succeeded in obtaining a new solvatomorph pair with distinct $Fe^{III}Co^{II}$ and $Fe^{II}Co^{III}$ electronic states by controlling the

crystallization temperature of the charge transfer complex $\{[Fe(Tp)(CN)_3]_2[Co(vbik)_2]_2\}$ which displays a thermally-induced electron transfer in MeOH solution near room temperature. The PF_6·salts **3** and **4** are isostructural to the previously reported BF_4 salts, **1** and **2**. Compound **4** displays a thermal ETCST transition above room temperature in the same way as **2**. In contrast, **3** is blocked in the paramagnetic state like **1** by solid phase interactions. As we hypothesized, the paramagnetic state in **3** can be converted to a diamagnetic state (of lower volume) by application of moderate pressure. The synthetic strategy is thus worth to explore further in future to obtain new piezo-magnetic switches.

Importantly, the comparison of the two isostructural solvatomorph pairs allows to rationalize the impact of the solid-state interactions on the electron-transfer process with and without pressure application. In our previous work, we have described the effects of the solid phase interactions on the core structure and consequently on the ETCST properties of Fe_2Co_2 square complexes. This hypothesis is further supported by the present results: PF_6^- replacing BF_4^- bestows to **3** and **4** stronger intermolecular interactions leading to higher coordination sphere distortion of Co^{II} ion in **3** and of Co^{III} ion in **4**. This stabilizes **3** in paramagnetic state and destabilizes **4** in diamagnetic state. Indeed, on the one hand we have observed that the paramagnetic state in **3** is better stabilize than in **1** at ambient pressure since no transition is revealed by magnetic measurement at low scan rate (0.01 K/min). On the other hand, **4** has lower transition temperature ($T_{1/2}$ = 315 K) in comparison with **2** ($T_{1/2}$ = 325 K).

Under pressure, the difference of ETCST behaviors between **3** and **1** are largely amplified. The occurrence of a piezo-induced electron transfer in **3** requires a higher threshold pressure (0.32 GPa LT pressure) than for **1** (0.10 GPa LT pressure). Once again, this could also be related to the higher distortion of the Co^{II} ion in **3**, stabilizing the paramagnetic state. Moreover, the transition of **3** is shown to be partial with a maximum conversion of 50 % which contrast with the full transition in **1**. This cannot be fully explained at this stage and may require better crystallographic data. Compound **3** shows a thermal hysteresis under pressure with a broader width. This might be correlated to the enhanced intermolecular interactions involving PF_6^- counter-anion and blocking ligands vbik and Tp. Interestingly the hysteresis width decreases upon pressure increase in **3**, in contrast with **1**. This might be related to their different distortion patterns of the core structures upon pressure application and its impact on the elastic interaction that promote cooperative transition. More accurate crystallographic data at 200 K would be required to evaluate the elastic properties of the compound **3** to further rationalize this behavior. Finally, an additional atypical feature of **3** is the regime change of the thermal ETCST at a critical pressure, above which a back-conversion from diamagnetic species to paramagnetic one takes place. This has been correlated to the occurrence of a crystal phase transition that is evidenced by both crystallographic and Raman spectroscopy data. To sum up, the magnetic properties of the two solvatomorph pairs unambiguously result from their specific solid-phase intermolecular interactions. Some features can be rationalized: pressure threshold to promote the electron transfer, atypical behavior due to a phase transition, larger hysteresis width associated with stronger intermolecular interactions. However, there is a clear need for the determination of the elastic properties of the material to allow an in-depth analysis on the structural origin. This is a challenging experimental task and such studies remain scarce in literature. However, we are convinced such approach can be fruitful and we are currently studying related compounds that are robust enough under pressure to allow the obtention of accurate pressure dependent structural data.

Experimental section

Synthesis and characterization of 3 and 4

The building bloc, $NBu_4[Fe^{III}(Tp)(CN)_3]$, was prepared according to the procedure described in the literature.[56] A mixture of $CoCl_2·6H_2O$ (23.7 mg, 0.1 mmol) and vbik (42.4 mg, 0.2 mmol) was dissolved in a 10 ml methanolic solution. Then a 15 ml methanolic solution containing $NBu_4[Fe^{III}(Tp)(CN)_3]$ (59 mg, 0.1 mmol) and a methanolic solution of NBu_4PF_6 (77 mg, 0.2 mmol) were added subsequently to the previous solution at 50 °C. The resulting orange-red solution was stirred at this temperature in water bath for 20 minutes, then filtered. Red square-like crystals (**3**) were obtained in a few days with a yield of 50 % by slow evaporating the solvent at *ca*. 40°C on a sand bath. Elemental analysis calcd (%) for $C_{68}H_{60}B_2Co_2Fe_2N_{34}O_4F_{12}P_2$ (characterized solvent: $2H_2O$ and MeOH) is that C: 40,89; H: 3.38; N: 23.50; Found: C: 40.26; H: 3.27; N: 23.37. Characteristic peaks in transmission FTIR spectrum (KBr pellet, figure S1a): 2508 cm^{-1} (ν_{B-H}), 2166 cm^{-1} (ν_{C-N}), 2126 cm^{-1} (ν_{C-N}), 2077 cm^{-1} (ν_{C-N}), 1648 cm^{-1} (ν_{C-O}), 896 cm^{-1} (ν_{PF6}). If the crystallization temperature is kept at 5°C in fridge, the same mother solution gives green square-like crystals (**4**) in a few days with a yield of 50 %. Elemental analysis calcd (%) for $C_{68}H_{60}B_2Co_2Fe_2N_{34}O_4F_{12}P_2$ (extra characterized solvent: one MeOH and $15H_2O$) is that C: 36.64; H: 4.07; N: 21.37; Found: C: 36.66; H: 4.19; N: 21.06. FTIR (KBr, cm^{-1}): Characteristic peaks in transmission FTIR spectrum (KBr pellet, figure S1b): 2502 cm^{-1} (ν_{B-H}), 2126 cm^{-1} (ν_{C-N}), 2077 cm^{-1} (ν_{C-N}), 1648 cm^{-1} (ν_{C-O}), 896 cm^{-1} (ν_{PF6}).

High-pressure (HP) Magnetic measurements.

Variable-temperature magnetization under different hydrostatic pressures was measured on a Quantum Design MPMS-XL7 SQUID magnetometer at a magnetic field of 1T. In a typical experiment, 5-7 mg of crystalline powder are placed in an HMD high-pressure cell made of hardened beryllium bronze, together with Daphne 7373 oil as the pressure transmitting medium (PTM) and a small piece of pure lead (Pb) wire as a pressure sensor. The sample, PTM and lead are introduced into a Teflon tube with an external diameter of 2.6 mm and a length of 7 mm inserted in the central cylinder of the HP cell. The tube is sealed with two Teflon caps. The critical temperature of the superconducting lead, T_c at 7.198 K before pressure application, shifts downward with increasing pressure in the range of 7.20-6.80 K. The applied pressure, *p*, is measured by the shift of T_c according to the following equation.

$$p = - \Delta Tc / 0.379 \text{ GPa}$$

The experimental error of the pressure measurement is estimated to be 0.02 GPa between 6.8 K - 7.20 K. However, the pressure increases with the temperature of the system, and could reach a value 0.1-0.15 GPa higher at room temperature.[42]

HP-μ Raman measurements on single crystal at 200 K

They were recorded using an argon laser operating at 514.5 nm and the spectra were collected in the spectral range of 700-2667 cm^{-1}. A single crystal of **3** was loaded in a Le Toullec - type membrane diamond anvil cell (DAC) with diamond culets of 600 μm in diameter and helium gas as the pressure transmitting medium. The sample chamber consisted of a rhenium gasket that was pre-indented to 60 μm, and then drilled by an fs Nd: YAG pulsed laser to make a 300 μm hole. The sample was loaded in the DAC together with a ruby sphere as a pressure sensor, and the measured temperature was decreased to 200 K by a helium continuous flow cryostat. The pressure values were determined by the fluorescence spectrum shift of the ruby, using the calibration of Shen et *al*.[57]

X-ray diffraction on single crystal at 200 K and ambient pressure

A single crystal (SC0) was selected, mounted and transferred into a cold nitrogen gas stream. Intensity data was collected with a Bruker Kappa APEX II system using fine-focus sealed tube Mo-Kα radiation (**3**) or micro-source Cu-Kα radiation (**4**). Unit-cell parameters determination, data collection strategy, integration and absorption correction were carried out with the Bruker APEX2 suite of programs. The structure was solved with SHELXT and refined anisotropically by full-matrix least-squares methods with SHELXL using WinGX. All structures were deposited at the Cambridge Crystallographic Data Centre with numbers CCDC 2265639-2265640 and can be obtained free of charge via www.ccdc.cam.ac.uk.

X-ray diffraction on single crystal under pressure at 300 K.

The HP-SC-XRD measurements were carried out at 300 K on two single crystals named SC1 and SC2 respectively. The crystal was loaded in diamond anvil cell in a stainless-steel gasket pre-indented at 100 μm with small ruby chips to probe the pressure and Daphnee oil 7474 as pressure transmitting media.[58] X-ray diffraction was measured on a Bruker D8 Venture diffractometer equipped with a molybdenum microfocus X-ray tube (Mo Kα radiation, λ=0.71073Å), the mirror optics as a monochromator, and a PHOTON III CMOS detector of size 10 x 14 cm. A short collimator and long beamstop were used as described by Vijayakumar-Symala et al 2022.[59]
The data integration and reduction were carried out using SAINT after excluding the shadowed regions with a dynamic mask.[60,61] An empirical absorption correction based on the intensities was performed by using SADABS. The atomic coordinates of the structure determined under ambient conditions were used as the starting model for the refinement of the crystal structure with data collected under pressure. Due to the poor completeness (~30%) H were constrained to be at the neutron tabulated value and some extra constraints were applied on certain atomic distances for SC2 (see table S1 for details). The structures under various pressure were deposited at the Cambridge Crystallographic Data Centre with numbers CCDC n° 2353837 (SC1, p = 0.62GPa), n° 2353844 (SC1, p = 0.76GPa), CCDC n° 2355116-2355120 (SC2, p = 0.96, 0.71, 0.43, 0.11 and 0.05 GPa respectively).

Author Contributions

All authors have contributed equally to the writing of the manuscript and given approval to the final version.

Conflicts of interest

There are no conflicts to declare.

Acknowledgements

We thank the GuangZhou Elite Project Scholars Association for awarding a three-year grant to Xu Buqin and the PMD2X X-ray diffraction facility of CRM2 laboratory (Université de Lorraine) for X-ray diffraction measurements (https://crm2.univ-lorraine.fr/plateformes/pmd2x/).

Notes and references

1. 1. K. Senthil Kumar, M. Ruben, Emerging trends in spin crossover (SCO) based functional materials and devices. *Coordination Chemistry Reviews* **346**, 176–205 (2017).

2. G. Molnár, S. Rat, L. Salmon, W. Nicolazzi, A. Bousseksou, Spin Crossover Nanomaterials: From Fundamental Concepts to Devices. *Advanced Materials* **30**, 1703862 (2018).

3. M. D. Manrique-Juarez, F. Mathieu, V. Shalabaeva, J. Cacheux, S. Rat, L. Nicu, T. Leïchlé, L. Salmon, G. Molnár, A. Bousseksou, A Bistable Microelectromechanical System Actuated by Spin-Crossover Molecules. *Angew Chem Int Ed* **56**, 8074–8078 (2017).

4. B. Benaicha, K. V. Do, A. Yangui, N. Pittala, A. Lusson, M. Sy, G. Bouchez, H. Fourati, C. J. Gómez-García, S. Triki, K. Boukheddaden, Interplay between spin-crossover and luminescence in a multifunctional single crystal iron(II) complex: towards a new generation of molecular sensors. *Chem. Sci.* **10**, 6791–6798 (2019).

5. K. S. Kumar, M. Ruben, Sublimable Spin-Crossover Complexes: From Spin-State Switching to Molecular Devices. *Angewandte Chemie International Edition* **60**, 7502–7521 (2021).

6. D. Aguilà, Y. Prado, E. S. Koumousi, C. Mathonière, R. Clérac, Switchable Fe/Co Prussian blue networks and molecular analogues. *Chem. Soc. Rev.* **45**, 203–224 (2015).

7. C. Mathonière, Metal-to-Metal Electron Transfer: A Powerful Tool for the Design of Switchable Coordination Compounds. *European Journal of Inorganic Chemistry* **2018**, 248–258 (2018).

8. T. Shiga, N. Mihara, M. Nihei, Cyanide-bridged assemblies with tricyanometalates. *Coordination Chemistry Reviews* **472**, 214763 (2022).

9. T. Mahfoud, G. Molnár, S. Bonhommeau, S. Cobo, L. Salmon, P. Demont, H. Tokoro, S.-I. Ohkoshi, K. Boukheddaden, A. Bousseksou, Electric-Field-Induced Charge-Transfer Phase Transition: A Promising Approach Toward Electrically

Switchable Devices. *J. Am. Chem. Soc.* **131**, 15049–15054 (2009).

10. G. N. Newton, M. Nihei, H. Oshio, Cyanide-Bridged Molecular Squares – The Building Units of Prussian Blue. *European Journal of Inorganic Chemistry* **2011**, 3031–3042 (2011).

11. M. Nihei, Molecular Prussian Blue Analogues: From Bulk to Molecules and Low-dimensional Aggregates. *Chem. Lett.* **49**, 1206–1215 (2020).

12. Y. Zhang, D. Li, R. Clérac, M. Kalisz, C. Mathonière, S. M. Holmes, Reversible Thermally and Photoinduced Electron Transfer in a Cyano-Bridged Fe2Co2 Square Complex. *Angewandte Chemie International Edition* **49**, 3752–3756 (2010).

13. J. Mercurol, Y. Li, E. Pardo, O. Risset, M. Seuleiman, H. Rousselière, R. Lescouëzec, M. Julve, [FeIILSCoIIILS]2 ⇔ [FeIIILSCoIIHS]2 photoinduced conversion in a cyanide-bridged heterobimetallic molecular square. *Chem. Commun.* **46**, 8995–8997 (2010).

14. M. Nihei, Y. Sekine, N. Suganami, K. Nakazawa, A. Nakao, H. Nakao, Y. Murakami, H. Oshio, Controlled Intramolecular Electron Transfers in Cyanide-Bridged Molecular Squares by Chemical Modifications and External Stimuli. *J. Am. Chem. Soc.* **133**, 3592–3600 (2011).

15. Y.-Z. Zhang, P. Ferko, D. Siretanu, R. Ababei, N. P. Rath, M. J. Shaw, R. Clerac, C. Mathoniere, S. M. Holmes, Thermochromic and Photoresponsive Cyanometalate Fe/Co Squares: Toward Control of the Electron Transfer Temperature. *J. Am. Chem. Soc.* **136**, 16854–16864 (2014).

16. C. Zheng, J. Xu, Z. Yang, J. Tao, D. Li, Factors Impacting Electron Transfer in Cyano-Bridged {Fe2Co2} Clusters. *Inorg. Chem.* **54**, 9687–9689 (2015).

17. S. Kamilya, S. Ghosh, S. Mehta, A. Mondal, Effect of Ligand Modulation on Metal-to-Metal Electron Transfer in a Series of [Fe2Co2] Molecular Square Complexes. *J. Phys. Chem. A* **125**, 4775–4783 (2021).

18. C.-Q. Jiao, Y.-S. Meng, Y. Yu, W.-J. Jiang, W. Wen, H. Oshio, Y. Luo, C.-Y. Duan, T. Liu, Effect of Intermolecular Interactions on Metal-to-Metal Charge Transfer: A Combined Experimental and Theoretical Investigation. *Angewandte Chemie International Edition* **58**, 17009–17015 (2019).

19. L. Meng, Y.-F. Deng, Y.-Z. Zhang, Anion-Dependent Electron Transfer in the Cyanide-Bridged [Fe2Co2] Capsules. *Inorg. Chem.* **60**, 14330–14335 (2021).

20. Y. Sekine, M. Nihei, H. Oshio, Dimensionally Controlled Assembly of an External Stimuli-Responsive [Co2Fe2] Complex into Supramolecular Hydrogen-Bonded Networks. *Chemistry – A European Journal* **23**, 5193–5197 (2017).

21. M. Nihei, Y. Yanai, I.-J. Hsu, Y. Sekine, H. Oshio, A Hydrogen-Bonded Cyanide-Bridged [Co2Fe2] Square Complex Exhibiting a Three-Step Spin Transition. *Angewandte Chemie International Edition* **56**, 591–594 (2017).

22. M. Nihei, Y. Yanai, D. Natke, R. Takayama, M. Kato, Y. Sekine, F. Renz, H. Oshio, Solid-State Hydrogen-Bond Alterations in a [Co2Fe2] Complex with Bifunctional Hydrogen-Bonding Donors. *Chemistry – A European Journal* **25**, 7449–7452 (2019).

23. L. Cao, J. Tao, Q. Gao, T. Liu, Z. Xia, D. Li, Selective on/off switching at room temperature of a magnetic bistable {Fe2Co2} complex with single crystal-to-single crystal transformation via intramolecular electron transfer. *Chem. Commun.* **50**, 1665–1667 (2014).

24. P. Gütlich, V. Ksenofontov, A. B. Gaspar, Pressure effect studies on spin crossover systems. *Coordination Chemistry Reviews* **249**, 1811–1829 (2005).

25. A. B. Gaspar, G. Molnár, A. Rotaru, H. J. Shepherd, Pressure effect investigations on spin-crossover coordination compounds. *Comptes Rendus Chimie* **21**, 1095–1120 (2018).

26. V. Ksenofontov, G. Levchenko, S. Reiman, P. Gütlich, A. Bleuzen, V. Escax, M. Verdaguer, Pressure-induced electron transfer in ferrimagnetic Prussian blue analogs. *Phys. Rev. B* **68**, 024415 (2003).

27. K. Boukheddaden, E. D. Loutete-Dangui, E. Codjovi, M. Castro, J. A. Rodriguéz-Velamazán, S. Ohkoshi, H. Tokoro, M. Koubaa, Y. Abid, F. Varret, Experimental access to elastic and thermodynamic properties of RbMnFe(CN)6. *Journal of Applied Physics* **109**, 013520 (2011).

28. J.-D. Cafun, J. Lejeune, F. Baudelet, P. Dumas, J.-P. Itié, A. Bleuzen, Room-Temperature Photoinduced Electron Transfer in a Prussian Blue Analogue under Hydrostatic Pressure. *Angewandte Chemie International Edition* **51**, 9146–9148 (2012).

29. A. Mondal, Y. Li, M. Seuleiman, M. Julve, L. Toupet, M. Buron-Le Cointe, R. Lescouezec, On/Off Photoswitching in a Cyanide-Bridged {Fe2Co2} Magnetic Molecular Square. *J. Am. Chem. Soc.* **135**, 1653–1656 (2013).

30. S. Kamilya, S. Ghosh, Y. Li, P. Dechambenoit, M. Rouzières, R. Lescouëzec, S. Mehta, A. Mondal, Two-Step Thermoinduced Metal-to-Metal Electron Transfer and ON/OFF Photoswitching in a Molecular [Fe_2Co_2] Square Complex. *Inorg. Chem.* **59**, 11879–11888 (2020).

31. S. De, J.-R. Jimenez, Y. Li, L.-M. Chamoreau, A. Flambard, Y. Journaux, A. Bousseksou, R. Lescouezec, One synthesis: two redox states. Temperature-oriented crystallization of a charge transfer {Fe2Co2} square complex in a {(FeLSCoLSIII)-Co-II}(2) diamagnetic or {(FeLSCoHSII)-Co-III}(2) paramagnetic state. *RSC Adv.* **6**, 17456–17459 (2016).

32. Y. Li, A. Benchohra, B. Xu, B. Baptiste, K. Béneut, P. Parisiades, L. Delbes, A. Soyer, K. Boukheddaden, R. Lescouëzec, Pressure-Induced Conversion of a Paramagnetic FeCo Complex into a Molecular Magnetic Switch with Tuneable Hysteresis. *Angewandte Chemie* **132**, 17425–17429 (2020).

33. B. Xu, Y. Li, B. Baptiste, L.-M. Chamoreau, D. Paliwoda, S. Mi, G. Molnár, K. Boukheddaden and R. Lescouëzec, *Chem. Mater.*, **36**, 8990-9001 (2024)

34. P. R. Spackman, M. J. Turner, J. J. McKinnon, S. K. Wolff, D. J. Grimwood, D. Jayatilaka, M. A. Spackman, CrystalExplorer: a program for Hirshfeld surface analysis, visualization and quantitative analysis of molecular crystals. *J Appl Cryst* **54**, 1006–1011 (2021).

35. M. A. Spackman, D. Jayatilaka, Hirshfeld surface analysis. *Crystengcomm* **11**, 19–32 (2009).

36. K. Ridier, A. Mondal, C. Boilleau, O. Cador, B. Gillon, G. Chaboussant, B. Le Guennic, K. Costuas, R. Lescouëzec, Polarized Neutron Diffraction to Probe Local Magnetic Anisotropy of a Low-Spin Fe(III) Complex. *Angewandte Chemie International Edition* **55**, 3963–3967 (2016).

37. E. Pardo, M. Verdaguer, P. Herson, H. Rousselière, J. Cano, M. Julve, F. Lloret, R. Lescouëzec, Synthesis, Crystal Structures, and Magnetic Properties of a New Family of Heterometallic Cyanide-Bridged FeIII2MII2 (M = Mn, Ni, and Co) Square Complexes (2011). https://doi.org/10.1021/ic200616p.

38. D. Li, R. Clérac, O. Roubeau, E. Harté, C. Mathonière, R. Le Bris, S. M. Holmes, Magnetic and Optical Bistability Driven by Thermally and Photoinduced Intramolecular Electron Transfer in a Molecular Cobalt−Iron Prussian Blue Analogue. *J. Am. Chem. Soc.* **130**, 252–258 (2008).

39. F. Lloret, M. Julve, J. Cano, R. Ruiz-García, E. Pardo, Magnetic properties of six-coordinated high-spin cobalt(II) complexes: Theoretical background and its application. *Inorganica Chimica Acta* **361**, 3432–3445 (2008).

40. V. Escax, G. Champion, M. A. Arrio, M. Zacchigna, C. C. D. Moulin, A. Bleuzen, The Co ligand field: A key parameter in photomagnetic CoFe Prussian blue derivatives. *Angew. Chem.-Int. Edit.* **44**, 4798–4801 (2005).

41. V. Ksenofontov, G. Levchenko, S. Reiman, P. Gütlich, A. Bleuzen, V. Escax, M. Verdaguer, Pressure-induced electron transfer in ferrimagnetic Prussian blue analogs. *Phys. Rev. B* **68**, 024415 (2003).

42. K. Yokogawa, K. Murata, H. Yoshino, S. Aoyama, Solidification of High-Pressure Medium Daphne 7373. *Jpn. J. Appl. Phys.* **46**, 3636 (2007).

43. S. F. A. Kettle, E. Diana, E. M. C. Marchese, E. Boccaleri, P. L. Stanghellini, The vibrational spectra of the cyanide ligand revisited: the ν(CN) infrared and Raman spectroscopy of Prussian blue and its analogues. *J Raman Spectroscopy* **42**, 2006–2014 (2011).

44. M. Ptak, A. Sieradzki, M. Šimėnas, M. Maczka, Molecular spectroscopy of hybrid organic–inorganic perovskites and related compounds. *Coordination Chemistry Reviews* **448**, 214180 (2021).

45. G. Molnár, V. Niel, A. B. Gaspar, J.-A. Real, A. Zwick, A. Bousseksou, J. J. McGarvey, Vibrational Spectroscopy of Cyanide-Bridged, Iron(II) Spin-Crossover Coordination Polymers: Estimation of Vibrational Contributions to the Entropy Change Associated with the Spin Transition. *J. Phys. Chem. B* **106**, 9701–9707 (2002).

46. R. Li, G. Levchenko, F. J. Valverde-Muñoz, A. B. Gaspar, V. V. Ivashko, Q. Li, B. Liu, M. Yuan, H. Fylymonov, J. A. Real, Pressure Tunable Electronic Bistability in Fe(II) Hofmann-like Two-Dimensional Coordination Polymer [Fe(Fpz)2Pt(CN)4]: A Comprehensive Experimental and Theoretical Study. *Inorg. Chem.* **60**, 16016–16028 (2021).

47. T. Matsuda, X. Liu, T. Shibata, H. Kamioka, Y. Ohishi, Y. Moritomo, Pressure-Induced Phase Transition in Zn–Fe Prussian Blue Lattice. *J. Phys. Soc. Jpn.* **78**, 105002 (2009).

48. M. M. Barsan, I. S. Butler, J. Fitzpatrick, D. F. R. Gilson, High-pressure studies of the micro-Raman spectra of iron cyanide complexes: Prussian blue ($Fe_4[Fe(CN)_6]_3$), potassium ferricyanide ($K_3[Fe(CN)_6]$), and sodium nitroprusside ($Na_2[Fe(CN)_5(NO)]\cdot 2H_2O$). *J Raman Spectroscopy* **42**, 1820–1824 (2011).

49. F. Guillermo Díaz, V. Marcelo Campos, A. Hugo Klahn O., Vibrational study of hydrotris(pyrazolyl)borato complexes of rhenium(I) tricarbonyl. *Vibrational Spectroscopy* **9**, 257–264 (1995).

50. S. De, A. Flambard, B. Xu, L.-M. Chamoreau, G. Gontard, L. Lisnard, Y. Li, M.-L. Boillot, R. Lescouëzec, Molecular Magnetic Materials Based on {CoIII(Tp*)(CN)3}− Cyanidometallate: Combined Magnetic, Structural and 59Co NMR Study. *Chemistry – A European Journal* **28**, e202200783 (2022).

51. J. Glatz, J.-R. Jiménez, L. Godeffroy, H. J. von Bardeleben, L. Fillaud, E. Maisonhaute, Y. Li, L.-M. Chamoreau, R. Lescouëzec, Enlightening the Alkali Ion Role in the Photomagnetic Effect of FeCo Prussian Blue Analogues. *J. Am. Chem. Soc.* **144**, 10888–10901 (2022).

52. M. Sy, F. Varret, K. Boukheddaden, G. Bouchez, J. Marrot, S. Kawata and S. Kaizaki, *Angew Chem Int Ed*, 2014, **53**, 7539–7542.

53. K. Murata, H. Yoshino, H. O. Yadav, Y. Honda, N. Shirakawa, Pt resistor thermometry and pressure calibration in a clamped pressure cell with the medium, Daphne 7373. *Review of Scientific Instruments* **68**, 2490–2493 (1997).

54. D. Staško, J. Prchal, M. Klicpera, S. Aoki, K. Murata, Pressure media for high pressure experiments, Daphne Oil 7000 series. *High Pressure Research* **40**, 525–536 (2020).

55. A. B. Jain, S. K. Deb, A. K. Tyagi, High pressure Raman spectroscopic study of phase transformations in Zn(CN)2. *Chemical Physics Letters* **758**, 137947 (2020).

56. R. Lescouëzec, J. Vaissermann, F. Lloret, M. Julve, M. Verdaguer, Ferromagnetic Coupling between Low- and High-Spin Iron(III) Ions in the Tetranuclear Complex fac-{[FeIII{HB(pz)3}(CN)2(μ-CN)]3FeIII(H2O)3}· 6H2O ([HB(pz)3]- = Hydrotris(1-pyrazolyl)borate). *Inorg. Chem.* **41**, 5943–5945 (2002).

57. G. Shen, J. S. Smith, C. Kenney-Benson, S. Klotz, Calibration of ruby (Cr3+:Al2O3) and Sm2+:SrFCl luminescence lines from the melting of mercury: constraints on the initial slopes. *High Pressure Research* **41**, 175–183 (2021).

58. K. Murata, K. Yokogawa, H. Yoshino, S. Klotz, P. Munsch, A. Irizawa, M. Nishiyama, K. Iizuka, T. Nanba, T. Okada, Y. Shiraga, S. Aoyama, Pressure transmitting medium Daphne 7474 solidifying at 3.7 GPa at room temperature. *Review of Scientific Instruments* **79**, 085101 (2008).

59. V. Vijayakumar-Syamala, E. Aubert, M. Deutsch, E. Wenger, A. Dhaka, M. Fourmigué, M. Nespolo, E. Espinosa, *N* -Iodosaccharin–pyridine co-crystal system under pressure: experimental evidence of reversible twinning. *Acta Crystallogr B Struct Sci Cryst Eng Mater* **78**, 436–449 (2022).

60. Bruker, 2019. APEX3. Version 2019.11. Bruker AXS Inc., Madison, Wisconsin, USA.

61. A. Dawson, D. R. Allan, S. Parsons, M. Ruf, Use of a CCD diffractometer in crystal structure determinations at high pressure. *J Appl Crystallogr* **37**, 410–416 (2004).